Vortex filament stability and boundary layer dynamics

Henry D. I. Abarbanel
Department of Physics, Institute for Nonlinear Science and Marine Physical Laboratory, Scripps Institution of Oceanography, University of California, San Diego, Mail Code 0402, La Jolla, California 92093-0402

A. Garrett Lisi
Department of Physics and Institute for Nonlinear Science, University of California, San Diego, Mail Code 0402, La Jolla, California 92093-0402

A. Rouhi and J. A. Wright
Institute for Nonlinear Science, University of California, San Diego, Mail Code 0402, La Jolla, California 92093-0402
(Received 7 January 1994)

Coherent structures in fluid boundary layers at high Reynolds numbers are a prominent feature of these flows. The structures appear as concentrations of vorticity into "hairpin" and other shapes. We explore the inviscid interaction and stability of vortex filaments initially situated spanwise to the mean flow in a model of a boundary layer. Both for a single vortex filament and its image through the boundary and for an infinite line of such filaments with their images we find a linear instability associated with deformations of the filament along its length with maximum instability having a wavelength on the order of the height of the filament above the boundary. The linear unstable manifold for this instability points at approximately 45° from the plane of the boundary in accord with experimental observations and numerical modeling of these coherent structures. This provides a dynamical origin to the observations of the orientation of these coherent structures.

PACS number(s): 47.32.Cc, 47.20.Cq, 47.27.Nz

I. INTRODUCTION

Coherent structures in boundary layer flows at high Reynolds number provide an attractive set of collective degrees of freedom with which one can anticipate describing the fluid dynamics on larger spatial scales [1,2]. An idealized model of the coherent structures is to consider them spanwise concentrations of vorticity which are generated near the wall in regions of the highest shear. The vortex filaments then distort and move according to their interaction with each other and with the background mean flow.

We have analyzed a simple model for the dynamics of these vortex filaments assuming they interact among themselves while moving in an inviscid background. To represent a boundary layer within this context we have studied both a single vortex filament and its image through the boundary and an infinite sequence of vortex filaments along the direction of the boundary and their images through the boundary. The two dimensional version of these arrangements is described by Lamb [3], and the consideration of three dimensional disturbances was carried out by Robinson and Saffman [4]. We have proceeded using a Hamiltonian formulation of the problem [5].

The key feature of this model of interacting vortex filaments, apparently unnoticed by Robinson and Saffman or Lamb before them, is that the direction of the unstable manifold for the vortex filaments lies approximately at a 45° tilt with respect to the streamwise direction and from the normal direction to the boundary. This angle is not precisely $\pi/4$ but is dynamically determined by the form of the instability and the angle we mention is for the most unstable modes. The angle for other modes varies in the vicinity of the angle for the maximum instability.

The precise value of the angle depends very weakly on the way in which the idealized, infinitely thin vortex filament is cut off to avoid its logarithmic self singularity [6]. In the case of a single filament and its image, as the cutoff we use varies over five orders of magnitude, the angle varies about 1° near a nominal mean of 43°.

There is clear experimental evidence for the importance of this approximate value for the tilt angle of vortices emergent in the turbulent boundary layer [7]. There is also striking numerical evidence from extensive large scale eddy simulations of the turbulent boundary layer that the direction of vorticity concentration is peaked near 45° [8]. The explanation for this given by Theodorsen [9] and discussed in detail by Head and Bandyopadhyay [7] is that the equation for the rate of change of the length of the vorticity vector has a term, the vortex stretching term, which depends on $\sin(2\theta)$, where θ is the angle in the plane normal to the direction of the filament. This term peaks at 45°, of course. As Head and Bandyopadhyay [7] then point out, there is no reason provided why the direction of maximum turbulence production, in the sense of vortex stretching and intensification, should be chosen by the system of vortex filaments as the primary direction of extension. In our calculation we demonstrate that the direction of the most unstable modes is $\theta \approx 43°$, and this provides the dynamical argu-

ment required to explain the observations.

There is an arbitrary distance introduced in this problem, namely the distance above the boundary (the x-z plane) at which the vortex filaments lie at the initial time. Since we do not have a model for the *production* of the filaments, we cannot hope to have an *a priori* reason for the choice of this distance. However, calling this distance $h/2$, we have determined that the instability arising from spanwise perturbations of the filament with wave number k_z with $hk_z \approx 0.5$ yields the maximum growth rate for the instability. From this an order of magnitude value of $h/2$ can be determined in the following way. As observed in experiments [7], the wavelength $\lambda_z = 2\pi/k_z$ associated with the spanwise separation of observed streamwise vorticity streaks is about $\lambda_z \approx 100$ in wall units, suggesting that the initial location of the vortex filament is about $h \approx \lambda_z/(4\pi) \approx 5-10$ in wall units. From the observations of Head and Bandyopadhyay [7] (as in their Figs. 28 and 30) we can see that this is the region of maximum shear $\partial u(y)/\partial y$ in their experiments. This is quite a natural place for the vortex filament to originate and gives further support to the physical picture in which vortex filaments are created near the wall in the region of maximum shear, and then through their own interaction and through the interaction with the mean flow they create the coherent structures [1,2] seen so clearly in observation. We are certainly not the first to suggest this picture [10,11,12], but we see substantial additional support for this view arising through the calculations we present in this paper.

It is natural to ask why a property of the *linear* instability of the vortex filament, namely the nearly 45° inclination of its unstable manifold, would have much to do with the observations. Our hypothesis, which we are now investigating by numerical simulations of the nonlinear regime, is that as the undulations of the filament move away from the wall from the very small value of $h \approx 5-10$ wall units where they are produced, the force on them from the image vortex, that is the effect of the wall, rapidly decreases, and they move very much as an isolated vortex filament through as inviscid fluid. Once launched at $\approx 45°$, they will continue in that direction interacting with themselves through induction among their own parts but all the while moving through the fluid at approximately the launch angle. Their own self interactions will distort the spanwise wave structures producing secondary instabilities which are seen in numerical simulations of the filament motion [11,13] as well as in experiments [7,10].

We shall consider first the case of a single filament and next an infinite array of filaments. In the latter case, when the filaments are even moderately well separated compared to their distance to the wall, the results are nearly identical to the single filament case.

II. SINGLE FILAMENT AND ITS IMAGE

A. General formulation

A vortex filament is a concentration of vorticity $\omega(\mathbf{x},t)$ along a line $\mathbf{R}(s,t)$ with s some labeling of the filament. We will consider a vortex filament which is located in the half space $y>0$ with a rigid boundary in the plane $y=0$ (see Fig. 1). Furthermore our filament will differ by a small amount from a perfectly straight filament aligned along the z axis. It is natural to label the filament by the coordinate z and specify the x and y locations of the filament by their z value at every time. This parameterization works locally all along the filament, and since we will be considering only small perturbations to filament along the z axis in this paper, it will be a quite adequate form for us. This means we write

$$\mathbf{R}(z,t)=(x(z,t),y(z,t),z)\ . \tag{1}$$

Since an initially straight filament will simply translate along the x direction with a constant velocity, it will be convenient to modify this form for $\mathbf{R}(z,t)$ slightly later on.

The vorticity field arising from a filament at $\mathbf{R}(z,t)$ around which the total circulation is Γ reads

$$\omega(\mathbf{x},t)=\Gamma\int_{-\infty}^{\infty} dz\,\delta^3(\mathbf{x}-\mathbf{R}(z,t))\frac{\partial \mathbf{R}(z,t)}{\partial z}\ . \tag{2}$$

The Hamiltonian for the interaction of vortices is just the kinetic energy of the fluid motion which results from the presence of the filament. The velocity $\mathbf{u}(\mathbf{x},t)$ due to the filament at $\mathbf{R}(z,t)$ is

$$\mathbf{u}(\mathbf{x},t)=\nabla\times\Psi(\mathbf{x},t)+\nabla\Phi(\mathbf{x},t)\ , \tag{3}$$

where

$$\Psi(\mathbf{x},t)=\frac{\Gamma}{4\pi}\int_{-\infty}^{\infty} dz\frac{\partial \mathbf{R}(z,t)}{\partial z}\frac{1}{|\mathbf{x}-\mathbf{R}(z,t)|} \tag{4}$$

is the vector potential due to a vortex filament in free space. In the presence of rigid boundaries, the term $\nabla\Phi$

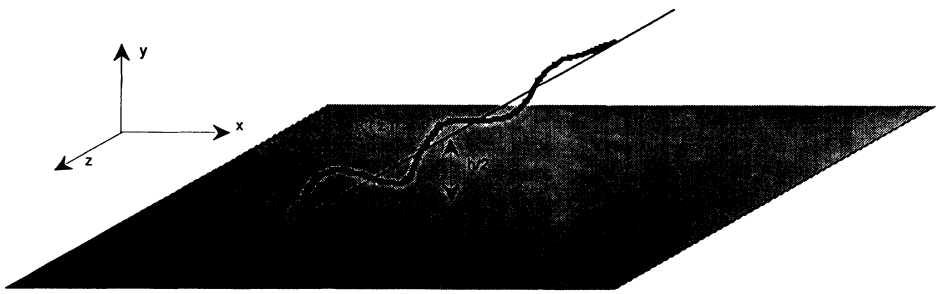

FIG. 1. A vortex filament of circulation Γ aligned along the z axis at a height $y=h/2$ above the x-z plane. Its image at $y=-h/2$ has circulation $-\Gamma$.

must be added so that the condition of vanishing normal velocity on the rigid surfaces can be satisfied. Incompressibility of the fluid means that

$$\nabla^2\Phi=0 , \tag{5}$$

while the boundary condition requires

$$\mathbf{n}\cdot\nabla\Phi=-\mathbf{n}\cdot\nabla\times\Psi , \tag{6}$$

where $\mathbf{n}$ is the unit normal to the boundary. This determines Φ.

In the problem of interest, the rigid boundary at $y=0$ is so simple that we may find an appropriate vector potential by the method of images. The free slip boundary condition at $y=0$ may be satisfied by an image filament with equal and opposite circulation located at

$$\mathbf{R}_I(z,t)=(x(z,t),-y(z,t),z) . \tag{7}$$

The resultant total velocity field of the fluid, located at $y>0$ is simply given by

$$\mathbf{u}(\mathbf{x},t)=\nabla\times\Psi(\mathbf{x},t) , \tag{8}$$

with Ψ now the vector potential due to the filament *and* its image:

$$\Psi(\mathbf{x},t)=\frac{\Gamma}{4\pi}\int_{-\infty}^{\infty}dz\frac{\partial\mathbf{R}(z,t)}{\partial z}\frac{1}{|\mathbf{x}-\mathbf{R}(z,t)|} -\frac{\Gamma}{4\pi}\int_{-\infty}^{\infty}dz\frac{\partial\mathbf{R}_I(z,t)}{\partial z}\frac{1}{|\mathbf{x}-\mathbf{R}_I(z,t)|} . \tag{9}$$

As noted above, the appropriate Hamiltonian for this problem is just the kinetic energy, given by

$$H=\tfrac{1}{2}\int d^3x\ \mathbf{u}(\mathbf{x},t)\cdot\mathbf{u}(\mathbf{x},t) =\tfrac{1}{2}\int d^3x\ \omega(\mathbf{x},t)\cdot\Psi(\mathbf{x},t) , \tag{10}$$

where an integration by parts is performed. A boundary term arising from the integration by parts vanishes. In the Hamiltonian above, Eq. (10), we use the vorticity given in Eq. (2) and the vector potential in Eq. (9).

Since we wish to investigate the stability of the steady state that consists of a perfectly straight filament uniformly translating along the x direction, it is convenient to slightly modify the coordinates $x(z,t)$ and $y(z,t)$, by writing

$$\mathbf{R}(z,t)=\left[Ut+x(z,t) , \frac{h}{2}+y(z,t) , z\right] , \tag{11}$$

where U is a constant translation velocity induced by the interaction between the filament and its image located at

$$\mathbf{R}_I(z,t)=\left[Ut+x(z,t) , \frac{-h}{2}-y(z,t) , z\right] . \tag{12}$$

$h/2$ is the distance of the unperturbed filament from the wall. For a vortex filament of circulation Γ, $U=\Gamma/2\pi h$ [3]. The steady motion is given by $\mathbf{R}(z,t)=(Ut,h/2,z)$ and $\mathbf{R}_I(z,t)=(Ut,-h/2,z)$; $x(z,t)$ and $y(z,t)$ will be the small quantities in our expansion.

Because we have shifted to a moving frame, expressed by the explicit time dependence which now appears in $\mathbf{R}(z,t)$, a term must be added to the Hamiltonian which generates this shift. The modified Hamiltonian will now be

$$H=\tfrac{1}{2}\int d^3x\ \omega(\mathbf{x},t)\cdot\Psi(\mathbf{x},t)-UP_x , \tag{13}$$

where P_x is the linear momentum of the fluid [5] in the x direction, given by

$$P_x=\Gamma\int dz\, y(z) . \tag{14}$$

With all this we may explicitly write the Hamiltonian in terms of the $(x(z,t),y(z,t))$ variables,

$$H=\frac{\Gamma^2}{8\pi}\int_{-\infty}^{\infty}dz\,dz'\left\{\frac{[x'(z,t)x'(z',t)+y'(z,t)y'(z',t)+1]}{[(x(z,t)-x(z',t))^2+(y(z,t)-y(z',t))^2+(z-z')^2+\mu^2]^{1/2}} -\frac{[x'(z,t)x'(z',t)-y'(z,t)y'(z',t)+1]}{[(x(z,t)-x(z',t))^2+(h+y(z,t)+y(z',t))^2+(z-z')^2]^{1/2}}\right\}-U\Gamma\int dz\, y(z,t) , \tag{15}$$

where the prime on $x(z,t)$ and $y(z,t)$ means derivative with respect to the z or z' label. To remove the logarithmic singularity which arises from the interaction of a vortex filament with itself, we use the simple expedient of adding a term μ^2 in the distance appearing in the denominator of the Hamiltonian [6]. The cutoff μ enters only in the first term, which is the self interaction of the filament and the self interaction of the image filament. A cutoff is not required in the second term, which represents the interaction of the filament with its image, that is, with the wall.

Clearly one can employ more realistic cutoff methods which reflect substantial physics about the structure of the filament "core," but since we will focus on instabilities which satisfy $k_z\mu\ll 1$, the precise value of this cutoff and the precise form of this cutoff are not of physical interest. Fortunately, the properties of the instability of interest near $k_zh\approx 0.5$ are weakly dependent on μ over many orders of magnitude of its value, so we can henceforth set aside the detailed nature of the cutoff.

The Hamiltonian (15) gives rise to equations of motion for the dynamical variables $x(z,t)$ and $y(z,t)$, which happen to be canonical with this method of labeling the filament. The Poisson bracket among the $x(z,t)$ and the

$y(z,t)$ are simply

$$\{x(z,t),y(z',t)\}=\frac{1}{\Gamma}\delta(z-z') . \tag{16}$$

The equations of motion resulting from these brackets are

$$\begin{aligned}\frac{\partial x(z',t)}{\partial t}&=\frac{1}{\Gamma}\frac{\delta H[x(z,t),y(z,t)]}{\delta y(z',t)} ,\\ \frac{\partial y(z',t)}{\partial t}&=-\frac{1}{\Gamma}\frac{\delta H[x(z,t),y(z,t)]}{\delta x(z',t)} ,\end{aligned} \tag{17}$$

where functional derivatives are used.

B. Small perturbations

We want to establish the form of the Hamiltonian which arises when the deviations $x(z,t)$ and $y(z,t)$ are "small." Two notions of small are used: (i) small with respect to the only length in the problem, namely h, and (ii) small in the sense that the z wave number k_z associated with the perturbation never becomes much larger than the order of $1/h$. If this occurs and, in particular, if $k_z\mu$ is large, the dynamics of the core of the vortex filament becomes important. This does not concern us here as we are focusing on large scale motions and interactions of these filaments. Treatment of the core in detail and of the dynamics of the core when filaments come close is beyond this consideration of the stability of the setting we have established. In all cases we will consider $\mu/h \ll 1$ and seek quantities which are insensitive to the precise value of μ over a large range.

When we expand the Hamiltonian in this way, we arrive at the linear and quadratic terms

$$\begin{aligned}H[x(z,t),y(z,t)]=\frac{\Gamma^2}{8\pi}\int_{-\infty}^{\infty}dz\,dz'\Bigg\{&\frac{(x'(z,t)x'(z',t))+y'(z,t)y'(z',t)}{\eta}-\frac{1}{2}\frac{(x(z,t)-x(z',t))^2+(y(z,t)-y(z',t))^2}{\eta^3}\\ &-\frac{x'(z,t)x'(z',t)-y'(z,t)y'(z',t)}{\zeta}\\ &+\frac{1}{2}\frac{(x(z,t)-x(z',t))^2+(y(z,t)+y(z',t))^2}{\zeta^3}-\frac{3}{8}\frac{4h^2(y(z,t)+y(z',t))^2}{\zeta^5}\Bigg\}\\ &+\left[\frac{\Gamma}{2\pi h}-U\right]\Gamma\int_{-\infty}^{\infty}dz\,y(z,t) ,\end{aligned} \tag{18}$$

where

$$\eta^2=(z-z')^2+\mu^2 , \tag{19}$$

and

$$\zeta^2=(z-z')^2+h^2 . \tag{20}$$

A formally infinite constant has been dropped from this expression.

The only linear term in the canonical variables appearing in the expansion of the Hamiltonian is the last one with coefficient $\Gamma/2\pi h-U$. For a steady state one must put $U=\Gamma/2\pi h$ in agreement with our previous observations. To work with this Hamiltonian, we now Fourier transform the variables $x(z,t)$ and $y(z,t)$ in the z direction using

$$x(z,t)=\frac{1}{2\pi}\int_{-\infty}^{\infty}dk_z X(k_z,t)e^{ik_z z} \tag{21}$$

and

$$y(z,t)=\frac{1}{2\pi}\int_{-\infty}^{\infty}dk_z Y(k_z,t)e^{ik_z z} . \tag{22}$$

The Hamiltonian is now diagonalized in wave-number space and reads

$$\begin{aligned}&H[X(k_z,t),Y(k_z,t)]\\ &\quad=\frac{\Gamma^2}{8\pi^2}\int_{-\infty}^{\infty}dk_z\{A(k_z)|X(k_z,t)|^2\\ &\qquad+B(k_z)|Y(k_z,t)|^2\} ,\end{aligned} \tag{23}$$

with

$$A(k)=k^2[K_0(k\mu)-K_0(kh)]+\frac{1-khK_1(kh)}{h^2}-\frac{1-k\mu K_1(k\mu)}{\mu^2} , \tag{24}$$

and

$$\begin{aligned}B(k)&=k^2[K_0(k\mu)+K_0(kh)]\\ &\quad+\frac{khK_1(kh)-(kh)^2K_2(kh)-1}{h^2}-\frac{1-k_\mu K_1(k\mu)}{\mu^2} .\end{aligned} \tag{25}$$

The functions $K_\nu(w)$ are Bessel functions of the third kind.

The equations of motion are

$$\frac{\partial X(k_z,t)}{\partial t}=\frac{\Gamma}{4\pi}B(k_z)Y(k_2,t) , \tag{26}$$

and

$$\frac{\partial Y(k_z,t)}{\partial t} = -\frac{\Gamma}{4\pi} A(k_z) X(k_z,t) \ . \tag{27}$$

This means that

$$\frac{\partial^2 X(k_z,t)}{\partial t^2} = -\frac{\Gamma^2}{16\pi^2} A(k_z) B(k_z) X(k_z,t) \ , \tag{28}$$

so the motion at any wave number k_z is unstable when the product $A(k_z)B(k_z)$ is negative.

In Fig. 2 we display the value of the growth rate $\Gamma/4\pi[-A(k_z)B(k_z)]^{1/2}$ as a function of the cutoff parameter μ, expressed as $\log_{10}(\mu/h)$, and the dimensionless spanwise wave number k_z/h. Over more than five orders of magnitude in the ratio μ/h, the growth rate varies about a factor of 2. In the neighborhood of $\mu/h \approx 0.001$, where we will perform our subsequent calculations, we see that the maximum growth rate is found near $k_z h \approx 0.5$. This is easier to see in the projected contour plot of the same information in Fig. 3.

In Fig. 4 we show the growth rate $\sigma(k_z h)$ as a function of the dimensionless wave number for the domain of instability $\sigma(k_z h) > 0$. This curve is computed with $\mu/h = 0.001$. To see the sensitivity of the angle of the instability, namely the eigendirection associated with growth, we plot in Fig. 5 the angle θ_{MAX} at the $k_z h$ of maximum growth rate as a function of μ/h over a large range of values. Again we see the rather insensitive dependence of this angle of maximum growth on the cutoff parameter.

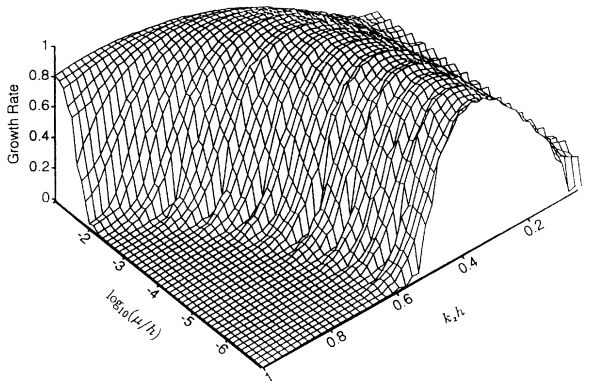

FIG. 2. Growth rate for a single vortex filament and its image initially located at $\pm h/2$ above and below the x-z plane. The growth rate is displayed as a function of the z (spanwise) wave number $k_z h$ and the cutoff size μ/h, which regularizes the logarithmic infinity of the self interaction of an infinitely thin filament. The dependence on μ/h is very weak. Only positive or zero growth rates, namely unstable or marginal modes, are shown.

Next we examine in Fig. 6 the actual angle associated with the linear instability as a function of $k_z h$ over the range of unstable wave numbers. To have some sense of the relative importance of these angles as might be seen in an arbitrary initial perturbation of the filament, which would possess all wave numbers with some distribution and would have no reason to be concentrated at the wave

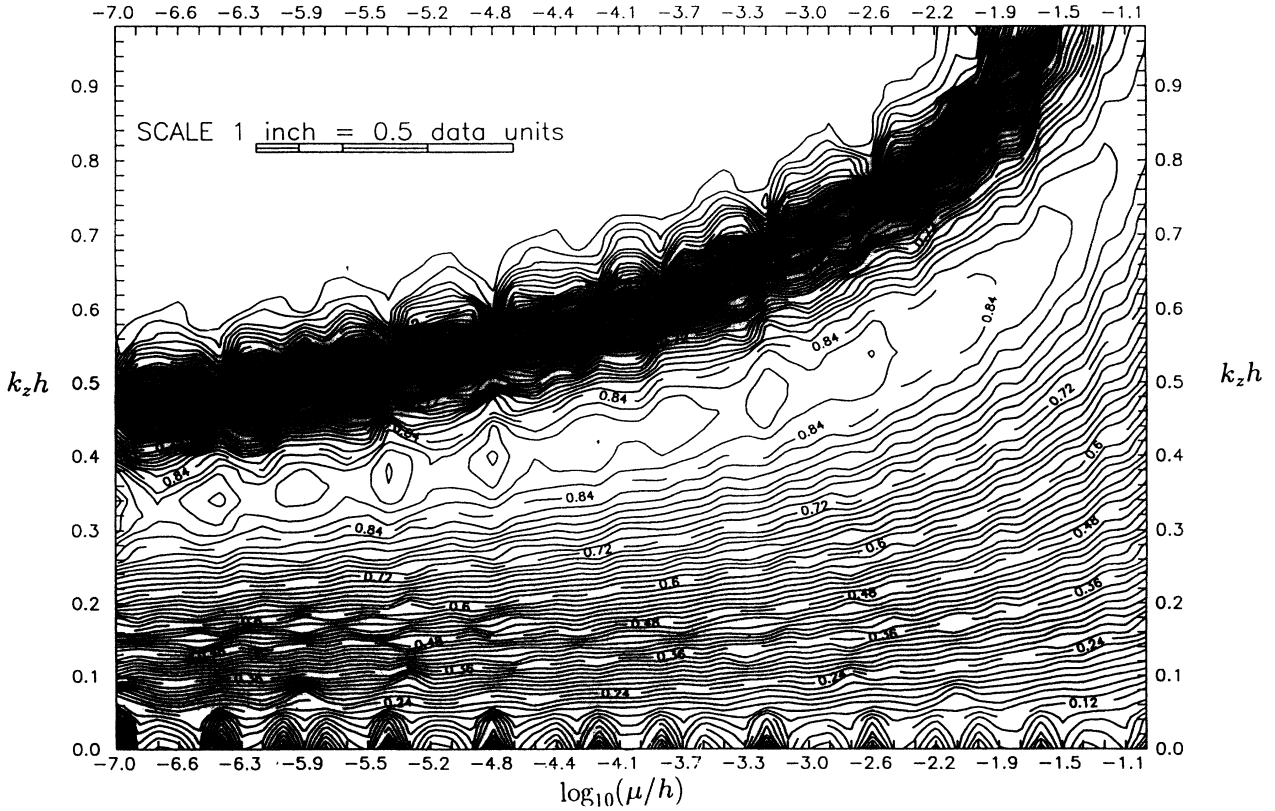

FIG. 3. The same information as displayed in Fig. 2 but shown as a contour plot. The ridge of maximum instability is rather insensitive to μ/h over many orders of magnitude of core size to filament height. The maximum growth rate is in the vicinity of $k_z h \approx 0.5$ for $\mu/h \approx 0.001$.

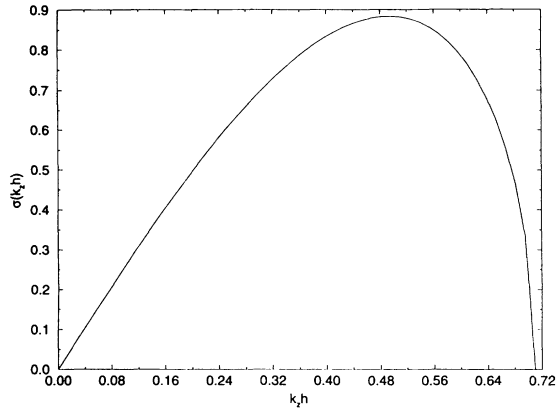

FIG. 4. The growth rate for a single filament and its image at $\pm h/2$ as a function of spanwise wave number $k_z h$. $\mu/h = 0.001$.

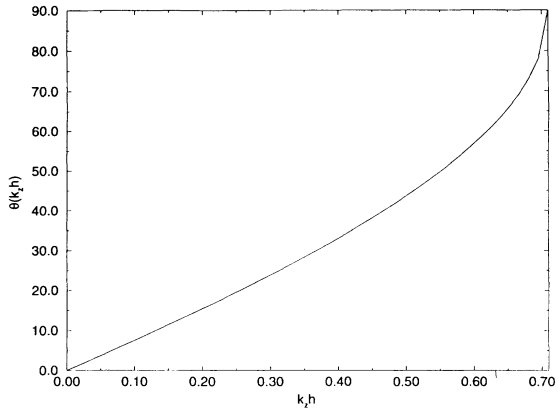

FIG. 6. The angle (deg) of the linear unstable manifold as a function of spanwise wave number $k_z h$ in the range of linear instability.

number of maximum growth rate, we show in Fig. 7 the angle of the unstable manifold plotted against the amount of growth e^{σ}. This is the magnitude of the increase of a perturbation in a "unit" time interval. Clearly the maximum growth occurs near 45°.

It bears repeating a comment noted in the Introduction that the value of the height h characterizing the initial location of the vortex filament is outside the model calculation we have presented. However, if we imagine that the filament develops primarily at the angle and spanwise wave number associated with the maximum growth rate of the instability and we associate wavelength of the most unstable mode with the remains of the filament which are left near the wall with the observed streamwise streaks typically separated by about 100 wall units, so $\lambda_z \approx 100$ in wall units [7], then we estimate that $h \approx 5$ in wall units. This is very close to the wall and as that is precisely where one expects the production mechanism to be dominant, the calculation is consistent within itself.

III. INFINITE LINEAR ARRAY OF VORTEX FILAMENTS

Now we turn to the situation where we have many vortex filaments interacting with each other but arranged so that each has its "image" in the x-z plane. We are modeling the dynamics of a boundary layer with many vortices above it [3]. The observations suggest that the boundary layer flow is dominated, at least in a visual sense, by a recurring set of vortex structures that are generated near the wall and then grow and advect downstream distorting into "horseshoe" shapes, which rise to substantial heights within the boundary layer. We do not yet have a realistic model of the formation of these vortices, though the general picture of highly shared flow rolling up through a Kelvin-Helmholtz type of instability is natural [12], so we do not address the origin of the vortex filaments in this paper. We also do not address their disappearance through viscosity or transport downstream, but remain with the tractable model of an infinite string of vortex filaments each starting a distance $h/2$ above the x-z plane ($y = 0$) and located an equal distance a from each other. Despite its unrealistic aspects, we anticipate that as more complicated and realistic models are built the overall essential features will remain. In any case this model allows us to easily assess the effect of the interaction of nearby vortices on the simple picture which emerged from the consideration of a single vortex filament above. We will find that as soon as the intervor-

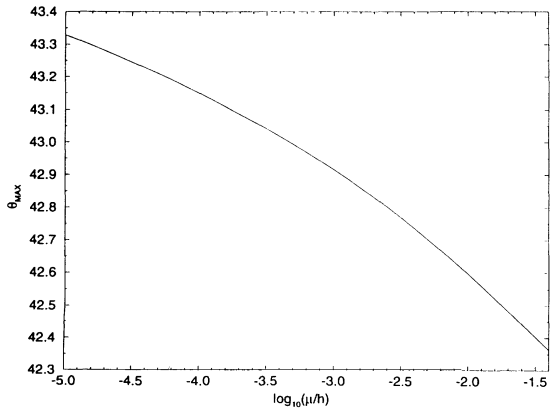

FIG. 5. The angle (deg) of the linear unstable manifold for the instability with maximum growth rate shown as a function of the cutoff or core size μ/h. The angle of maximum instability is nearly 43° as μ/h ranges over many orders of magnitude.

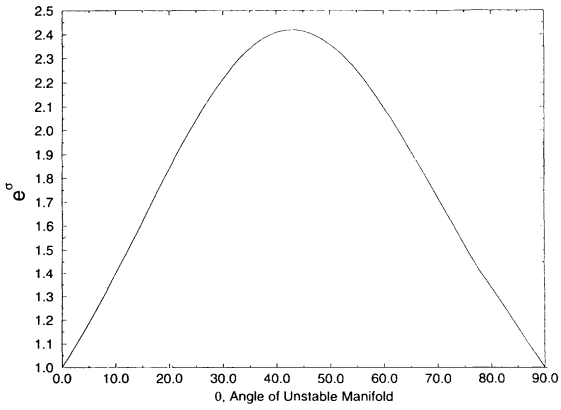

FIG. 7. Growth rate for unstable modes and the angle of inclination (deg) associated with the mode. Clearly the modes at angles near 45° grow substantially faster than others.

tex separation becomes even moderately large $a/h \geq 5$, there is little effect of one vortex on another in the region of instability. For closer vortices there is some effect, but until $a/h \leq 1$ the effect is small. From the discussion of Wallace [10] and from other indications from experiment and numerical calculations [14] it would appear that $a/h \approx 10$ to 20 is suggested. This would mean that the vortex filaments develop more or less independently interacting with the wall, as represented by their image, and with the background mean flow. The latter is not part of the present considerations, but we shall include it in our subsequent work.

A. General formulation

We now consider the Hamiltonian for a row of vortex filaments each with circulation Γ located at

$$\mathbf{R}_m(z,t)=(Ut+ma+x_m(z,t),h/2+y_m(z,t),z)\ , \tag{29}$$

namely near a height $h/2$ above the x-z plane. When the fields $x_m(z,t)$ and $y_m(z,t)$ are zero, we have uniform translation in the x direction of the whole row of vortices filaments at velocity U which we will determine below. The row starts with equal distance a between the filaments and this is maintained in the base state around which we will consider perturbations. Each vortex filament has an image with circulation $-\Gamma$ located at the sites

$$\mathbf{R}_k(z,t)=(Ut+ka+x_k(z,t),-h/2-y_k(z,t),z)\ . \tag{30}$$

The Hamiltonian divides into three parts composed of first, the self interaction of the vortex filaments together with interaction with filaments in the same row, second, the interaction between the vortex filaments and their images, and finally a piece proportional to the total x direction momentum, again generating a uniform translation U in the x direction. The net Hamiltonian for all of these terms is

$$\begin{aligned}
&H[x_n(z,t),y_j(z,t)] \\
&=\frac{\Gamma^2}{8\pi}\sum_{m,k=-\infty}^{\infty}\int_{-\infty}^{\infty}dz\,dz'\left\{\frac{[1+x_m'(z,t)x_k'(z',t)+y_m'(z,t)y_k'(z',t)]}{[(x_m(z,t)-x_k(z',t))^2+(y_m(z,t)-y_k(z',t))^2+(z-z')^2+\mu^2]^{1/2}}\right. \\
&\qquad\left.-\frac{[1+x_m'(z,t)x_k'(z',t)-y_m'(z,t)y_k'(z',t)]}{[(x_m(z,t)-x_k(z',t)+(m-k)a)^2+(y_m(z,t)+y_k(z',t)+h)^2+(z-z')^2]^{1/2}}\right\} \\
&\qquad -U\Gamma\sum_{m=-\infty}^{\infty}\int dz\,y_m(z,t)\ .
\end{aligned} \tag{31}$$

Again μ only appears in the interaction of the vortex filament with itself and in the interaction of its image with self. In analogy to the single filament case, the appropriate Poisson brackets are given by

$$\{x_m(z),y_n(z')\}=\frac{\delta_{nm}}{\Gamma}\delta(z-z')\ . \tag{32}$$

B. Small perturbations

This Hamiltonian is expanded about the steady solution $\mathbf{R}_m(z,t)=(Ut+ma,h/2,z)$ and for this we expand the integrand for H in $x_m(z,t),y_m(z,t)$ up to second order. This results in the expression

$$\begin{aligned}
&H[x_n(z,t),y_j(z,t)] \\
&=-U\Gamma\sum_{m=-\infty}^{\infty}\int dz\,y_m(z,t) \\
&\quad+\frac{\Gamma^2}{8\pi}\sum_{m,k=-\infty}^{\infty}\int_{-\infty}^{\infty}dz\,dz'\left\{\frac{x_m'(z,t)x_k'(z',t)+y_m'(z,t)y_k'(z',t)}{D(\mu)}\right. \\
&\qquad-\frac{1}{2}\frac{2a(m-k)(x_m(z,t)-x_k(z',t))+(x_m(z,t)-x_k(z',t))^2+(y_m(z,t)-y_k(z',t))^2}{D(\mu)^3} \\
&\qquad+\frac{3}{2}\frac{a^2(m-k)^2(x_m(z,t)-x_k(z',t))^2}{D(\mu)^5}-\frac{x_m'(z,t)x_k'(z',t)-y_m'(z,t)y_k'(z',t)}{D(h)} \\
&\qquad+\frac{1}{2}\frac{(x_m(z,t)-x_k(z',t))^2+(y_m(z,t)+y_k(z',t))^2}{D(h)^3} \\
&\qquad+\frac{h(y_m(z,t)+y_k(z',t))+a(m-k)(x_m(z,t)-x_k(z',t))}{D(h)^3} \\
&\qquad\left.-\frac{3}{2}\frac{(hy_m(z,t)+y_k(z',t))+a(m-k)(x_m(z,t)-x_k(z',t))^2}{D(h)^5}\right\}\ ,
\end{aligned} \tag{33}$$

with

$$D(w)=[(z-z')^2+(m-k)^2a^2+w^2]^{1/2}\ . \tag{34}$$

This Hamiltonian is diagonalized when we perform two transformations on the dynamical variables $x_m(z,t)$ and $y_m(z,t)$. First we introduce the Fourier transform in the variable z, as we did above. In addition, we introduce the Fourier transform on the finite domain $[0,a]$ to treat the discrete index m. The variable $x_m(z,t)$ has the expression

$$x_m(z,t)=\int_{-\infty}^{\infty}\frac{dk_z}{2\pi}\int_0^a\frac{d\xi}{a}\exp\left[\frac{2i\pi\xi m}{a}+ik_z z\right]x(k_z,\xi,t)\ , \tag{35}$$

and similarly for $y_m(z,t)$.

Using these coordinates, the Hamiltonian becomes diagonal:

$$\begin{aligned}
&H[x(k_z,\xi),y(k_z,\xi)]\\
&=\frac{\Gamma^2}{8\pi^2}\int_{-\infty}^{\infty}dk_z\int_0^a\frac{d\xi}{a}\left\{(|x(k_z,\xi)|^2+|y(k_z,\xi)|^2)\left[k_z^2\sum_{n=-\infty}^{\infty}\int_0^\infty dv\frac{\cos(k_z v)\cos\left[\frac{2\pi n\xi}{a}\right]}{\Delta(\mu)}\right.\right.\\
&\qquad\left.\left.-\sum_{n=-\infty}^{\infty}\int_0^\infty dv\frac{1-\cos(k_z v)\cos\left[\frac{2\pi n\xi}{a}\right]}{\Delta(\mu)^3}\right]\right.\\
&\qquad+3a^2|x(k_z,\xi)|^2\sum_{n=-\infty}^{\infty}n^2\int_0^\infty dv\frac{1-\cos(k_z v)\cos\left[\frac{2\pi n\xi}{a}\right]}{\Delta(\mu)^5}\\
&\qquad-k_z^2[|x(k_z,\xi)|^2-|y(k_z,\xi)|^2]\sum_{n=-\infty}^{\infty}\int_0^\infty dv\frac{\cos(k_z v)\cos\left[\frac{2\pi n\xi}{a}\right]}{\Delta(h)}\\
&\qquad+|x(k_z,\xi)|^2\sum_{n=-\infty}^{\infty}\int_0^\infty dv\frac{1-\cos(k_z v)\cos\left[\frac{2\pi n\xi}{a}\right]}{\Delta(h)^3}\\
&\qquad+|y(k_z,\xi)|^2\sum_{n=-\infty}^{\infty}\int_0^\infty dv\frac{1+\cos(k_z v)\cos\left[\frac{2\pi n\xi}{a}\right]}{\Delta(h)^3}\\
&\qquad-3h^2|y(k_z,\xi)|^2\sum_{n=-\infty}^{\infty}\int_0^\infty dv\frac{1+\cos(k_z v)\cos\left[\frac{2\pi n\xi}{a}\right]}{\Delta(h)^5}\\
&\qquad-3a^2|x(k_z,\xi)|^2\sum_{n=-\infty}^{\infty}n^2\int_0^\infty dv\frac{1-\cos(k_z v)\cos\left[\frac{2\pi n\xi}{a}\right]}{\Delta(h)^5}\\
&\qquad+3ahi(y^*(k_z,\xi)x(k_z,\xi)-y(k_z,\xi)x^*(k_z,\xi))\\
&\qquad\left.\times\sum_{n=-\infty}^{\infty}n\int_0^\infty dv\frac{\sin\left[\frac{2\pi n\xi}{a}\right]\cos(k_z v)}{\Delta(h)^5}\right\}\\
&+\left[\frac{2}{a}\Gamma\coth\left[\frac{\pi h}{a}\right]-U\right]\Gamma\sum_{n=-\infty}^{\infty}\int_{-\infty}^{\infty}dz\,y_n(z,t)\ ,
\end{aligned} \tag{36}$$

where

$$\Delta(w)=(w^2+v^2+n^2a^2)^{1/2} . \tag{37}$$

As in the single filament case, the last term is the only linear term; therefore we choose $U=2\Gamma\coth(\pi h/a)/a$ to have a steady state. This correctly picks out the translation velocity of a symmetric double array of line vortices [3]. The fact that the Hamiltonian is diagonalized in these coordinates clearly reflects the translational symmetry of the unperturbed state in the z direction and the periodicity of that state in the x direction.

The decomposition of the variables $x_m(z,t)$ and $y_m(z,t)$ differs slightly from that of Lamb [3], as followed by Robinson and Saffman [4]. They chose

$$x_m(z,t)=X(t)e^{[ik_z z+im\phi]} , \tag{38}$$

with a single value of ϕ across the row of vortex filaments. If the ξ integral were peaked near $\xi=\phi$, this would give a correct guess for the functional form of the displacement $x_m(z,t)$. To the extent that both Lamb and Robinson and Saffman were simply trying to establish the instability of the rows of vortex filaments, this choice is quite sufficient. To make the connection between the model and any observed phenomena in a boundary layer, we must explore the fuller space of possibilities. In fact, we will see that when the vortices in the row are quite close together, $a/h\approx 2$ or less, this simplified choice for the dependence on m is quite acceptable. When a/h becomes larger, even $a/h\approx 8$ is enough and the dependence on ξ among the unstable modes is quite smooth and without any dominant value of ξ so the m dependence of the vortex filaments is not $e^{im\phi}$. When we have near independence of ξ among the unstable modes, we are being told that the behavior is similar to that of an isolated vortex filament, which is quite sensible for large values of a/h as the interaction between filaments decreases rapidly as their distance increases.

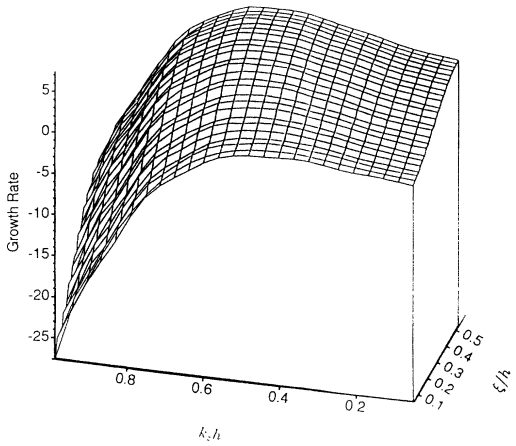

FIG. 8. Growth rate of a line of vortex filaments (and their images) as a function of the spanwise wave number $k_z h$ and the streamwise variation parameter ξ/h for initial separation of the filaments of $a/h=2$. There is some weak dependence on ξ/h visible in these calculations. $\mu/h=0.001$, here.

The Hamiltonian (36) can be written in the matrix form

$$H[x(k_z,\xi),y(k_z,\xi)]=\frac{\Gamma^2}{8\pi^2}\int_{-\infty}^{\infty}dk_z\int_0^a\frac{d\xi}{a}(x^*(k_z,\xi),y^*(k_z,\xi))\begin{bmatrix}A(k_z,\xi) & C(k_z,\xi)\\ C^*(k_z,\xi) & B(k_z,\xi)\end{bmatrix}\begin{bmatrix}x(k_z,\xi)\\ y(k_z,\xi)\end{bmatrix} , \tag{39}$$

where $C(k_z,\xi)$ is pure imaginary $C(k_z,\xi)=-C^*(k_z,\xi)$ and $A(k_z,\xi)$ and $B(k_z,\xi)$ are real. Fairly compact expressions can be given for these coefficients by performing the v integrations which give rise again to Bessel functions of the third kind. With the notation

$$\alpha_n=k_z(a^2n^2+\mu^2)^{1/2} \tag{40}$$

$$\beta_n=k_z(a^2n^2+h^2)^{1/2} , \tag{41}$$

$$S(c,a)=\frac{\pi}{ac}\coth\left[\frac{\pi c}{a}\right] , \tag{42}$$

$$T_{\pm}(c,a)=\frac{\pi}{a^2c}\left[\frac{a\cosh(\pi c/a)\sinh(\pi c/a)\pm\pi c}{\sinh^2(\pi c/a)}\right] , \tag{43}$$

we have

$$A(k_z,\xi)=S(h,a)-S(\mu,a)-T_-(h,a)+T_-(\mu,a)+\sum_{n=-\infty}^{\infty}\cos(2\pi in\xi)\left[\frac{\alpha_n^2K_0(\alpha_n)+\alpha_nK_1(\alpha_n)-a^2n^2k_z^2K_2(\alpha_n)}{a^2n^2+\mu^2}-\frac{\beta_n^2K_0(\beta_n)-\beta_nK_1(\beta_n)+a^2n^2k_z^2K_2(\beta_n)}{a^2n^2+h^2}\right] , \tag{44}$$

and

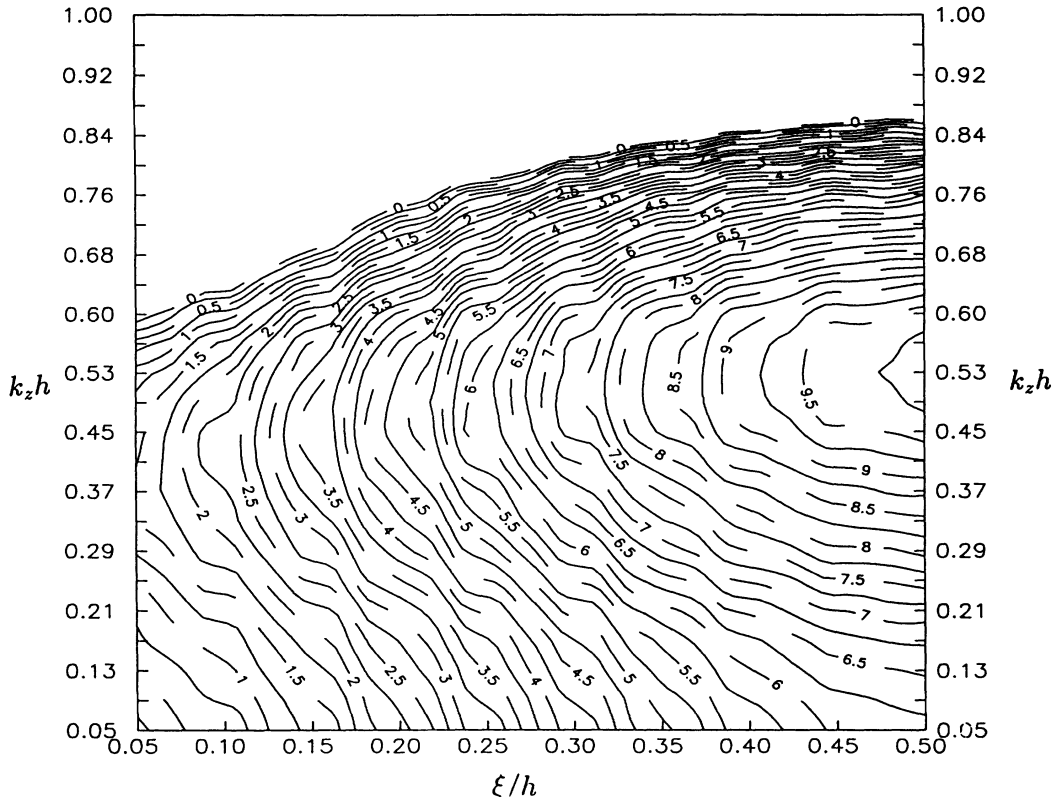

FIG. 9. A contour plot of the same information as in Fig. 8 with negative growth rates (stable modes) not displayed.

$$B(k_z,\xi)=S(h,a)-S(\mu,a)-T_+(h,a)$$

$$+\sum_{n=-\infty}^{\infty}\cos(2\pi i n\xi)\left[\frac{\alpha_n^2K_0(\alpha_n)+\alpha_nK_1(\alpha_n)}{a^2n^2+\mu^2}+\frac{\beta_n^2K_0(\beta_n)+\beta_nK_1(\beta_n)-h^2k_z^2K_2(\beta_n)}{a^2n^2+h^2}\right], \tag{45}$$

and finally

$$C(k_z,\xi)=-2iah\sum_{n=-\infty}^{\infty}\sin(2\pi i n\xi)\frac{nk_z^2K_2(\beta_n)}{a^2n^2+h^2}\ . \tag{46}$$

Using Eqs. (32) and (35) the Poisson brackets for the diagonalizing variables are

$$\{x(k_z,\xi),y^*(k_z',\xi')\}=\frac{2\pi a}{\Gamma}\delta(k_z-k_z')\delta(\xi-\xi')\ . \tag{47}$$

These Poisson brackets and the Hamiltonian (39) lead to the equations of motion

$$\begin{aligned}4\pi\Gamma\frac{\partial x(k_z,\xi,t)}{\partial t}&=-C(k_z,\xi)x(k_z,\xi,t)\\&\quad+B(k_z,\xi)y(k_z,\xi,t)\ ,\\4\pi\Gamma\frac{\partial y(k_z,\xi,t)}{\partial t}&=-A(k_z,\xi)x(k_z,\xi,t)\\&\quad-C(k_z,\xi)y(k_z,\xi,t)\ ,\end{aligned} \tag{48}$$

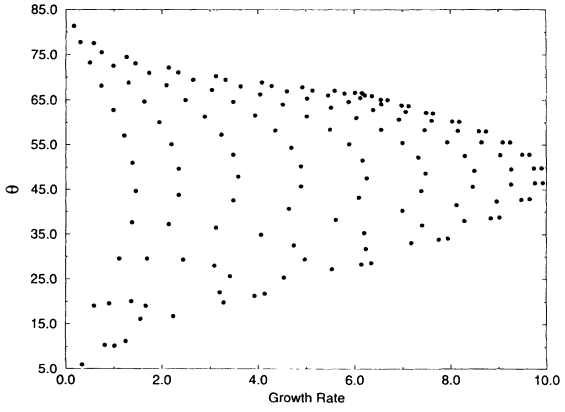

FIG. 10. The inclination angle (deg) of the linear unstable manifold for a line of vortex filaments with $a/h=2$. The sets of angles are associated with various values of $k_z h$ and ξ/h as seen in Fig. 8. An inclination angle of $\approx 45°$ is associated with the maximum growth rate in each case.

which tells us that the system is stable when $A(k_z,\xi)B(k_z,\xi)>0$.

We have analyzed the Hamiltonian for two choices of the ratio of the initial filament height above the plane h and the filament separation a. In Fig. 8 we present the growth rate for $a/h=2$ for $0.05\leq k_z h\leq 1.0$ and $0.05\leq\xi/h\leq 1.0$. Both negative (stable) and positive (unstable) growth rates are seen. In this computation we use $\mu=0.001$ and cut off the sums over the Bessel functions arising from the integrals over v in the expressions for $A(k_z,\xi)$ and $B(k_z,\xi)$ at index 10. Ten values were used in the ξ display and 20 in the k_z display. The same information is shown as a contour plot in Fig. 9 but here we have suppressed contours associated with negative growth rates. It is apparent that the growth rate is dependent, though not dramatically, on the value of ξ/h so the ansatz that the only variation of $x_m(z,t)$ would be as $e^{im\phi}$ would not be appropriate for such an initial filament spacing. In Fig. 10 we present the inclination angle of the linear unstable manifold for the line of vortex filaments with the same range of parameters as just indicated. The various curves of growth rate versus inclination angle are associated with varying values of $k_z h$ and ξ/h. The variation with ξ/h is apparent here.

In Fig. 11 we move on to an initial filament spacing $a/h=8$ and display the growth rate as a function of $k_z h$ and ξ/h. The dependence on ξ/h has essentially disappeared now, as one might expect for the rather isolated vortex filaments now in the problem. Figure 12 is the contour plot of this same information; again the negative growth rate contours have been suppressed. The rather substantial independence of the unstable modes on ξ/h is quite clear. Finally in Fig. 13 we have the inclination angle of the linear unstable manifold as a function of the growth rate. The close bunching of the values once again

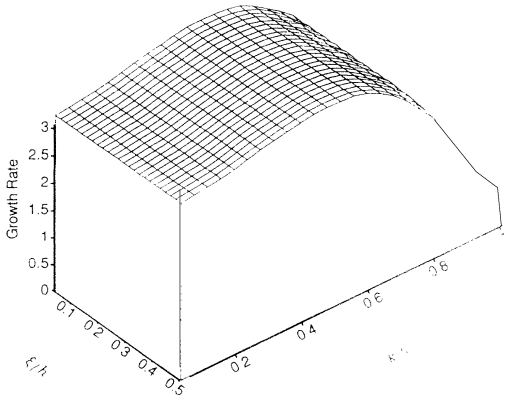

FIG. 11. Growth rate of a line of vortex filaments (and their images) as a function of the spanwise wave number $k_z h$ and the streamwise variation parameter ξ/h for initial separation of the filaments of $a/h=8$. There is little dependence on ξ/h visible in these calculations. $\mu/h=0.001$, here.

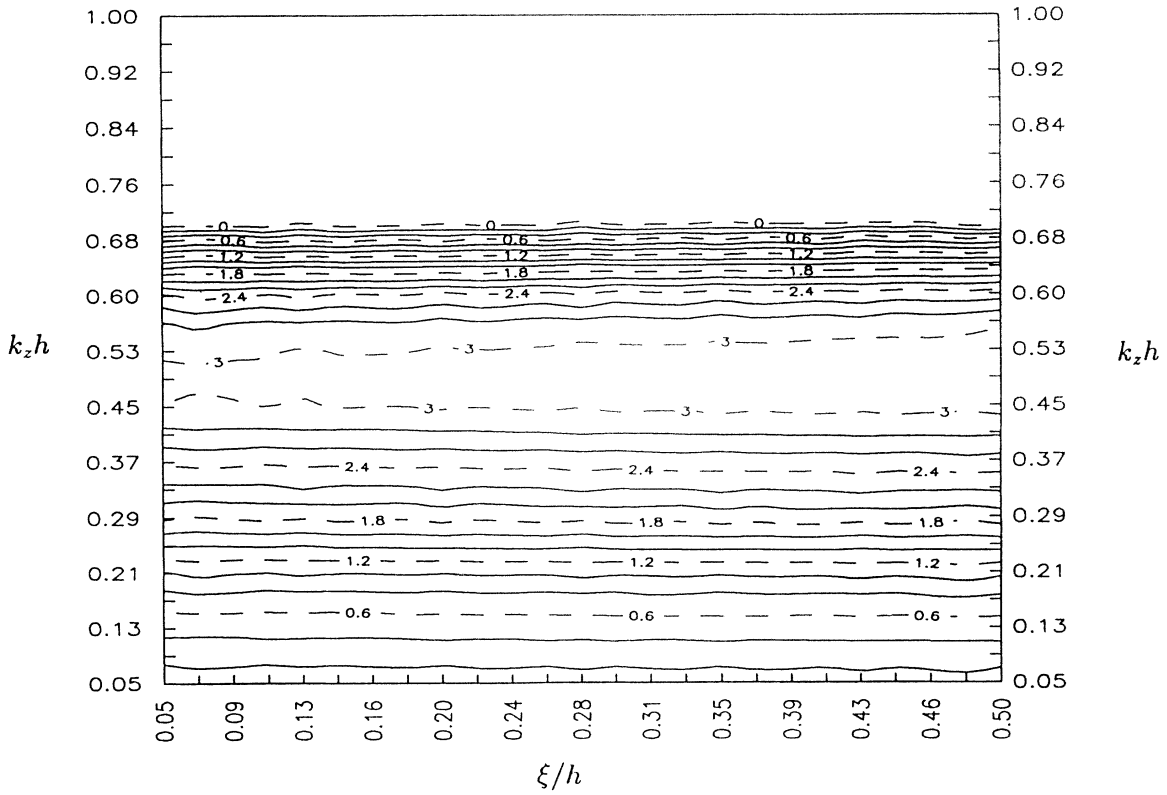

FIG. 12. A contour plot of the same information as in Fig. 11 with negative growth rates (stable modes) not displayed. Variation with ξ/h is nearly absent.

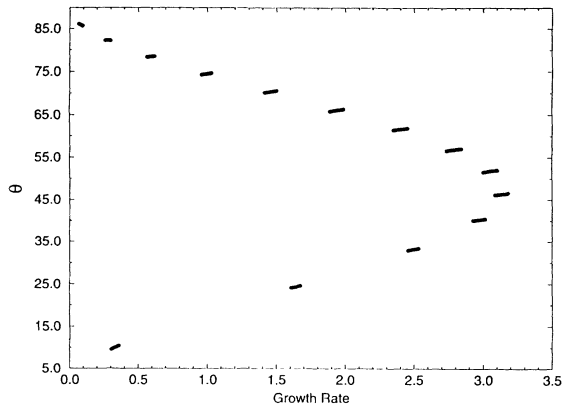

FIG. 13. The inclination angle (deg) of the linear unstable manifold for a line of vortex filaments with $a/h=8$. The sets of angles are associated with various values of $k_z h$ and ξ/h as seen in Fig. 11. An inclination angle of $\approx 45°$ is associated with the maximum growth rate in each case. The absence of variation with ξ/h is quite apparent.

reflects the independence of the solution at these larger values of a/h to ξ/h. The independence of variations on ξ/h means an ansatz of the kind discussed above would also not be appropriate here.

IV. CONCLUSIONS: BOUNDARY LAYER MODELS

The unified picture of concentrated spanwise vortex filaments generated near the wall in boundary layer flows (which then interact with each other and through an instability to spanwise fluctuations, rising through the boundary layer to be seen as hairpin vortices leaving trailing streamwise "legs") is hardly initiated in this paper. Many have suggested and analyzed the observed features of these flows within such a framework [9,10,12].

We have added to this discussion and quantitatively strengthened the value of such models by two main results.

(i) We have identified the approximate location of the height of the *generation* of the vortex filaments by associating the wavelength of the maximum spanwise instability with the observed separation between streamwise streaks. The maximum instability near $k_z h \approx 0.5$ leads to $h \approx 5-10$ in wall units when the spanwise wavelength $2\pi/k_z \approx 100$ in wall units.

(ii) We have identified the inclination angle of the linear unstable manifold of the most unstable spanwise modes, which is near 45° with the angle observed by many and found in extensive numerical simulations.

Absent from our computations is a mechanism for the generation of these vortex filaments. The origins of these filaments suggested by Corcos [15] and his co-workers seems natural. We have also not dealt with the effects of the background flow, though following Leonard [13] its incorporation is straightforward.

Our further explorations of this model will represent the generation of the vortex filaments as a nearly periodic process [12] taking place near the wall, $h \approx$ a few wall units, and then interacting with the images induced by the presence of the wall, with the other vortices and with the mean flow. Within this framework we anticipate that one can construct a rather complete picture of the generation, interaction, and evolution, and subsequent decay and disappearance of the vortical structures which dominate the boundary layer at high Reynolds number.

Part of our motivation for this exploration is the recent observation that when sensed with an instrument large compared to the scale of the coherent structures, one sees quite clearly only a few degrees of freedom dominating the boundary layer [16]. Almost certainly these are the reflection of a few coherent structures made visible by the averaging out of small scale fluctuations. One of our goals in these investigations is to produce a dynamical model based on vortex filament interaction which can be compared with the observations using the method of nonlinear dynamical analysis developed for these low dimensional problems [17].

ACKNOWLEDGMENTS

This work was supported in part by the U. S. Department of energy, Office of Basic Energy Sciences, Division of Engineering and Geosciences, under Contract No. DE-FG03-90ER14138, in part by the U.S. Army Research Office (Contract No. DAAL03-91-C-052), and by the Office of Naval Research (Contract No. N00014-91-C-0125), under subcontract to the Lockheed-Sanders Corporation. The research of A. Rouhi was supported by the U.S. Department of Energy, CHAMMP Program under Grant No. DE-FG03-91ER612222. A. G. Lisi was partially supported by the San Diego Chapter of the ARCS Foundation.

[1] B. J. Cantwell, Ann. Rev. Fluid Mech. **13**, 457 (1981).
[2] S. K. Robinson, Ann. Rev. Fluid Mech. **23**, 601 (1991).
[3] H. Lamb, *Hydrodynamics* (Cambridge University Press, Cambridge, England, 1932).
[4] A. C. Robinson and P. G. Saffman, J. Fluid Mech. **125**, 411 (1982).
[5] A. Rouhi and J. Wright, Phys. Rev. E **48**, 1850 (1993).
[6] P. G. Saffman, *Vortex Dynamics* (Cambridge University Press, New York, 1992).
[7] M. R. Head and P. Bandyopadhyay, J. Fluid Mech. **107**, 297 (1981).
[8] P. Moin and J. Kim, J. Fluid Mech. **155**, 441 (1985).
[9] T. Theodorsen (unpublished).
[10] J. M. Wallace, in *Developments in Theoretical and Applied Mechanics, XI,* edited by T. J. Chung and G. R. Karr (University of Alabama, Huntsville, 1982), pp. 509-521.
[11] T.-L. Hon and J. D. A. Walker, Comput. Fluids **20**, 343 (1991).
[12] W. W. Willmarth, Adv. Mech. **15**, 159 (1975).
[13] A. Leonard, J. Comput. Phys. **37**, 289 (1980).
[14] J. Jiménez, P. Moin, R. Moser, and L. Keefe, Phys. Fluids **31**, 1311 (1988).

[15] G. M. Corcos, in *The Role of Coherent Structures in Modelling Turbulence and Mixing,* edited by J. Jiménez, Lecture notes in Physics Vol. 136 (Springer-Verlag, Berlin, 1981).

[16] H. D. I. Abarbanel, J. Cembrola, T. Frison, T. Galib, and R. Katz, Phys. Rev. E **49**, 4003 (1994).

[17] H. D. I. Abarbanel, R. Brown, J. J. Sidorowich, and Lev Sh. Tsimring, Rev. Mod. Phys. **65**, 1331 (1993).

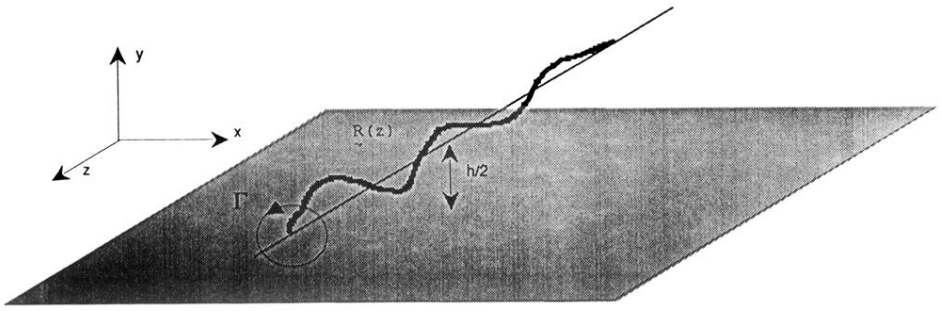

FIG. 1. A vortex filament of circulation Γ aligned along the z axis at a height $y=h/2$ above the x-z plane. Its image at $y=-h/2$ has circulation $-\Gamma$.

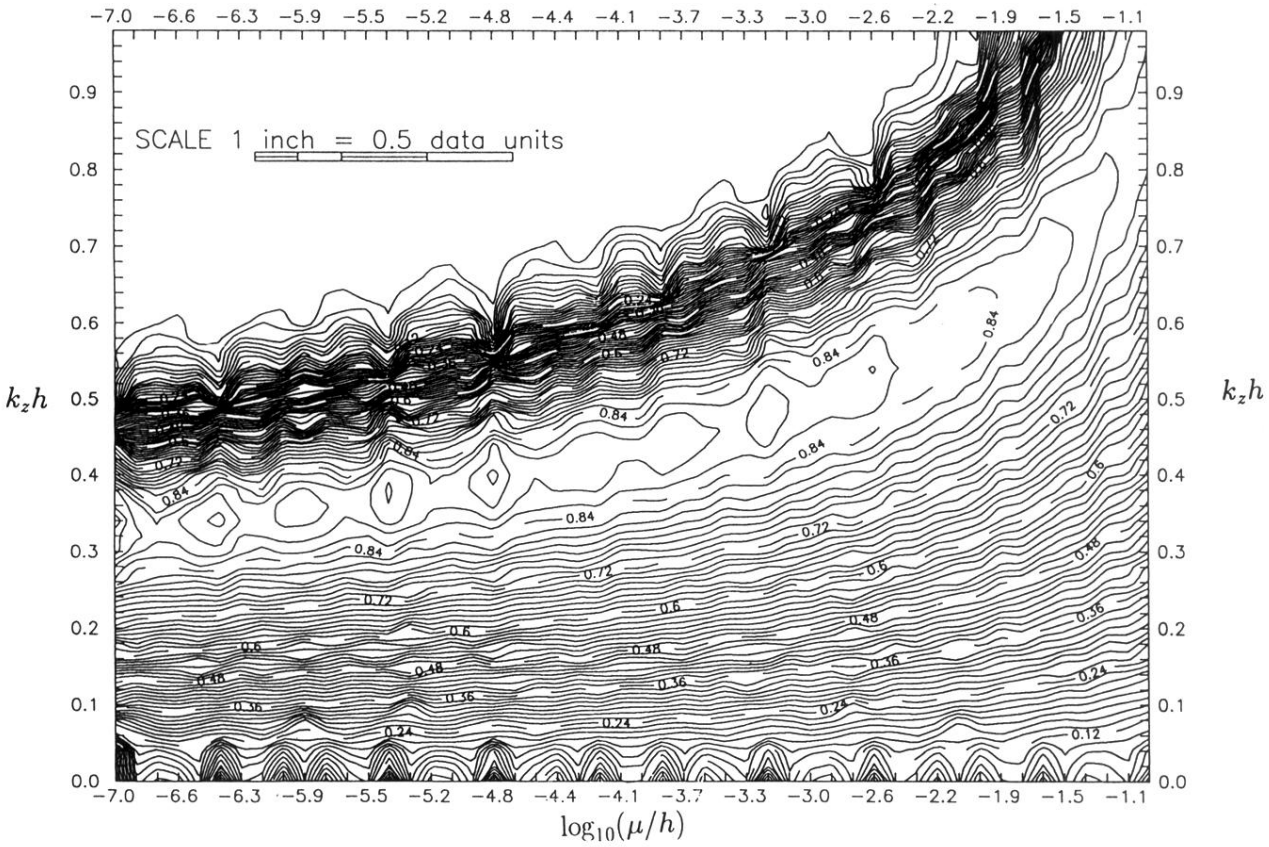

FIG. 3. The same information as displayed in Fig. 2 but shown as a contour plot. The ridge of maximum instability is rather insensitive to μ/h over many orders of magnitude of core size to filament height. The maximum growth rate is in the vicinity of $k_z h \approx 0.5$ for $\mu/h \approx 0.001$.